

Multifunctional Immunoliposomes Enhance the Immunotherapeutic Effects of PD-L1 Antibodies against Melanoma by Reprogramming Immunosuppressive Tumor Microenvironment

Yu Hei, Yang Chen, Qian Li, Zi Mei, Jijia Pan, Siqi Zhang, Chunyang Xiong,* Xiaodong Su,* and Shicheng Wei*

The immunosuppressive tumor microenvironment (TME) can significantly limit the immunotherapeutic effects of the PD-L1 antibody (aPDL1) by inhibiting the infiltration of CD8⁺ cytotoxic T cells (CTLs) into the tumor tissues. However, how to reprogram the immunosuppressive TME and promote the infiltration of CTLs remains a huge challenge for aPDL1 to achieve the maximum benefits. Herein, the authors design a multifunctional immunoliposome that encapsulates the adrenergic receptor blocker carvedilol (CAR) and connects the “don’t eat me” signal antibody (aCD47) and aPDL1 in series via a reactive oxygen species (ROS)-sensitive linker on the surface. In ROS-enriched immunosuppressive TME, the multifunctional immunoliposome (CAR@aCD47/aPDL1-SSL) can first release the outer aCD47 to block the “do not eat me” pathway, promote the phagocytosis of tumor cells by phagocytic cells, and activate CTLs. Then, the aPDL1 on the liposome surface is exposed to block the PD-1/PD-L1 signaling pathway, thereby inducing CTLs to kill tumor cells. CAR encapsulated in CAR@aCD47/aPDL1-SSL can block the adrenergic nerves in the tumor tissues and reduce their densities, thereby inhibiting angiogenesis in the tumor tissues and reprogramming the immunosuppressive TME. According to the results, CAR@aCD47/aPDL1-SSL holds an effective way to reprogram the immunosuppressive TME and significantly enhance immunotherapeutic efficiency of aPDL1 against the primary cancer and metastasis.

1. Introduction

The immunosuppressive tumor microenvironment (TME) is an essential factor of the antitumor response. How to reprogram the immunosuppressive TME remains a huge challenge for immunotherapy to achieve ideal benefits.^[1–3] The immunosuppressive TME can limit the immunotherapeutic effects of immune checkpoint blockades (ICBs), such as PD-L1 antibodies (aPDL1) and PD-1 antibodies, by inhibiting the infiltration of T lymphocytes into the tumor tissue.^[3] The immunosuppressive TME contains excessive amounts of reactive oxygen species (ROS), which are closely related to immunosuppressive responses and tumor development and progression.^[4–7] ROS act as signaling molecules in tumor tissues, contributing to tumor growth, metastasis, and resistance to apoptosis.^[8,9] Therefore, ROS scavenging in TME is expected to reprogram the immunosuppressive TME, promote the infiltration of T lymphocytes into tumor tissues, and enhance the antitumor therapeutic effect of ICBs.

Y. Hei, Z. Mei, S. Wei
Central Laboratory, and Department of Oral and Maxillofacial Surgery
School and Hospital of Stomatology
Peking University
Beijing 100081, P. R. China
E-mail: sc-wei@pku.edu.cn

Y. Hei, C. Xiong
Department of Mechanics and Engineering Science
College of Engineering
Peking University
Beijing 100871, P. R. China
E-mail: cyxiong@pku.edu.cn

Y. Chen, Q. Li, J. Pan, S. Wei
Laboratory of Biomaterials and Regenerative Medicine
Academy for Advanced Interdisciplinary Studies
Peking University
Beijing 100871, P. R. China

 The ORCID identification number(s) for the author(s) of this article can be found under <https://doi.org/10.1002/smll.202105118>.

S. Zhang
Institute of molecular medicine
Peking University
Beijing 100871, P. R. China

C. Xiong
Wenzhou Institute
University of Chinese Academy of Sciences
Wenzhou, Zhejiang 325000, P. R. China

C. Xiong
Oujiang Laboratory (Zhejiang Lab for Regenerative Medicine,
Vision and Brain Health)
Wenzhou, Zhejiang 325001, P. R. China

X. Su
Biomedical Pioneering Innovation Center (BIOPIC)
State Key Laboratory of Protein and Plant Gene Research,
School of Life Sciences
Peking University
Beijing 100871, P. R. China
E-mail: xdsu@pku.edu.cn

DOI: 10.1002/smll.202105118

In addition, the solid TME contains nerve fibers that arise from the peripheral nervous system.^[10,11] Recent research indicated that newly formed adrenergic nerve fibers could promote tumor angiogenesis and induce immunosuppression, thereby promoting tumor growth and metastasis.^[12] Clinical data indicated that carvedilol (CAR), a blocker of β receptors, can prolong the survival of patients by inhibiting the neoplastic adrenergic nerves.^[13,14] Therefore, CAR may have a synergistic therapeutic effect with ICBs by blocking the adrenergic nerve fibers and remodeling the immunosuppressive TME.

The integrin-associated protein CD47, a ligand of signal-regulatory protein- α (SIRP α), is upregulated on the surfaces of various malignant tumor cells.^[15,16] The CD47/SIRP α pathway, also called the “do not eat me” pathway, has been considered an important mechanism by which tumor cells evade innate immune surveillance.^[17,18] The antibody of CD47 (“don’t eat me” signal antibody [aCD47]) can activate phagocytic cells to phagocytize tumor cells and present relevant antigens to activate T lymphocytes.^[19–21] These results have provided a scientific rationale for investigating the use of aCD47 in enhancing the immunotherapy effect of CTLA-4 or PD-1/PD-L1 blockades.^[22–26]

The aPD-L1, an ICB, could block the tumor immunosuppressive signaling pathway PD-1/PD-L1 by specifically binding to the PD-L1 receptor, which is highly expressed on the surfaces of tumor cells.^[27–30] aPD-L1 has a good immunotherapy effect on some cancers in clinical applications, such as nonsmall cell lung cancer, head and neck cancer, and melanoma.^[30,31] However, the application of aPD-L1 is limited because of its unsatisfactory therapeutic effects and systemic side effects.^[32,33] As mentioned above, excessive ROS and adrenergic nerve fibers in transmission electron microscopy (TEM) and the “do not eat

me” pathway may be important limiting factors that cause the unsatisfactory therapeutic effects of aPD-L1. In addition, the systemic side effects of aPD-L1 may be related to its poor targeting ability in the body.^[32] Liposomes are ideal drug delivery vehicles, which can deliver a variety of drugs and enhance the targeting ability of drugs to the tumor tissues through the permeability and retention (EPR) effect.^[34,35] In our previous research, we found that binding aPD-L1 to a liposome surface for the preparation of an immunoliposome can enhance the tumor-targeting ability of aPD-L1 through the EPR effect and reduce its side effects.^[36]

Here, to reprogram the tumor suppressive microenvironment, enhance the antitumor effect of aPD-L1, and reduce its side effects, we constructed a multifunctional immunoliposome (CAR@aCD47/aPD-L1-SSL) (Figure 1a,b) encapsulating an adrenergic receptor blocker CAR, and connecting aCD47 and aPD-L1 in series via a ROS-sensitive linker (bis-*N*-hydroxy succinimide [NHS]-modified 2,2'-[propane-2,2-diylbis(thio)] diacetic acid) (Figure S1, Supporting Information) on the surface. The multifunctional immunoliposome (CAR@aCD47/aPD-L1-SSL) is expected to induce the ROS-responsive sequential release in the TME. We hypothesized that in ROS-enriched the immunosuppressive TME, the multifunctional immunoliposome (CAR@aCD47/aPD-L1-SSL) can first release the outer aCD47 to block the “do not eat me” pathway, promote the phagocytosis of tumor cells by phagocytic cells, and activate T lymphocytes. Then the aPD-L1 on the liposome surface is exposed to block the PD-1/PD-L1 signaling pathway, thereby promoting T lymphocytes to recognize and kill tumor cells. ROS-sensitive linkers can not only regulate the sequential release of antibodies on the liposome surface, but also

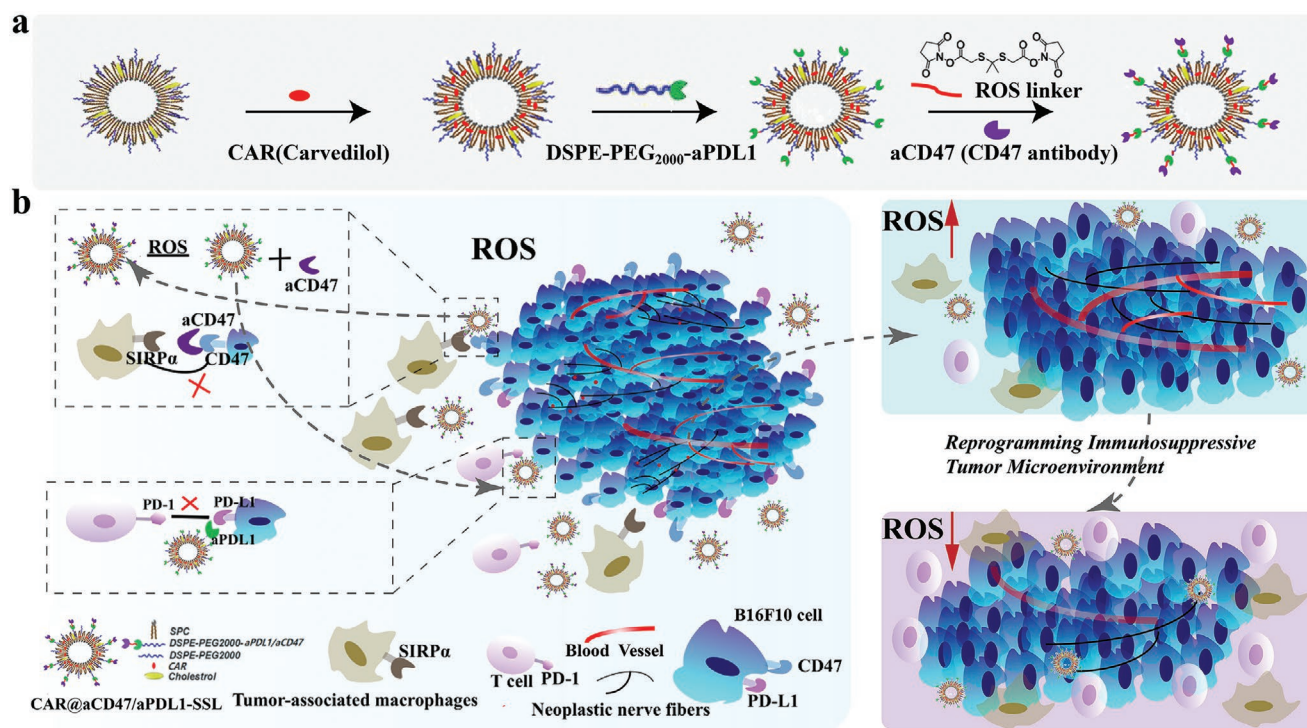


Figure 1. a) Schematic diagram of the structure and b) the antitumor mechanism of the multifunctional immunoliposome CAR@aCD47/aPD-L1-SSL.

scavenge ROS in the TME. Moreover, CAR encapsulated in liposomes can block tumor neoplastic adrenergic nerve fibers, thereby inhibiting angiogenesis in tumor tissues, reprogramming the immunosuppressive TME, promoting the infiltration of T lymphocytes into tumor tissues, and enhancing the effect of aPDL1. Thus, the multifunctional immunoliposome (CAR@aCD47/aPDL1-SSL) is expected to produce synergistic effects and enhance antitumor therapeutic effects through the controlled sequential release of aCD47 and aPDL1, downregulation of ROS signals, and inhibition of neoplastic adrenergic nerves in the TME.

2. Result and Discussion

2.1. Multifunctional Immunoliposomes Preparation and Characterization

To achieve the ROS-responsive sequential release of aCD47 and aPDL1, we first synthesized an ROS-sensitive linker

(bis-*N*-hydroxy succinimide [NHS]-modified 2,2'-[propane-2,2-diylbis (thio)] diacetic acid) (Figure S1, Supporting Information) and used it to connect aCD47 and aPDL1 in a series. Then, a multifunctional immunoliposome (CAR@aCD47/aPDL1-SSL) (Figure 1a,b) with the encapsulated CAR and tandem antibody on its surface was prepared with the thin film dispersion/postinsertion method. The average particle size of CAR@aCD47/aPDL1-SSL determined by dynamic light scattering (DLS) was 124 nm (PDI: 0.213). CAR@aCD47/aPDL1-SSL had an approximate spherical structure and good dispersion capabilities, as indicated by TEM (Figure 2b,e). The average particle size of CAR@aPDL1-SSL was 98 nm (PDI: 0.221), slightly smaller than that of CAR@aCD47/aPDL1-SSL (Figure 2a,d). The average particle size of CAR@aCD47/aPDL1-SSL was reduced to ≈ 101 nm in H_2O_2 solution, which was close to the particle size of CAR@aPDL1-SSL (Figure 2c,f). The possible reason was the release of aCD47 after the reaction of ROS-sensitive linkers with H_2O_2 and the resulting small liposome particle size. The zeta potentials of aPDL1-SSL and aCD47-SSL were -18.12 ± 0.87 and -22.33 ± 0.97 mV,

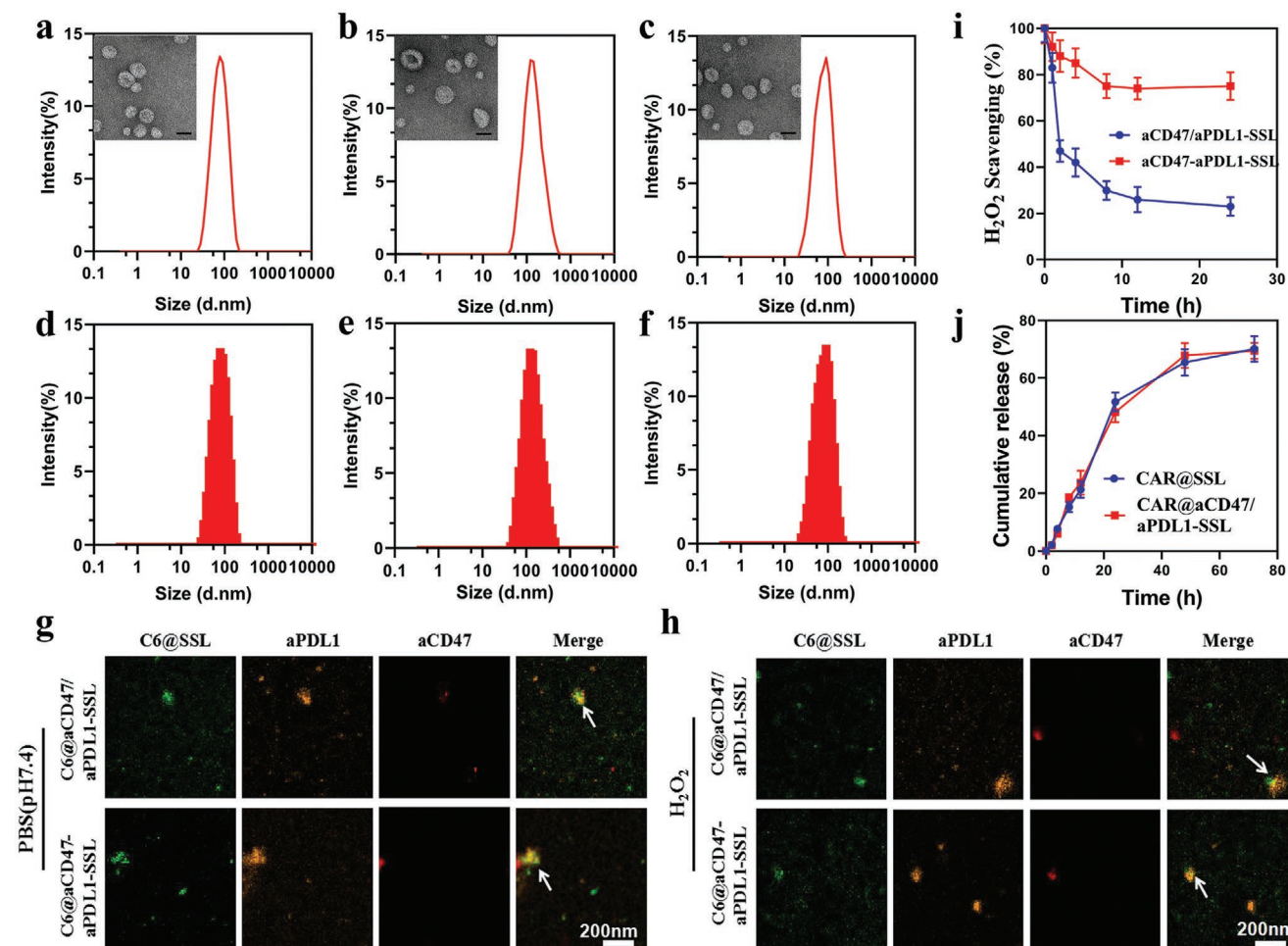


Figure 2. Characterization of CAR@aCD47/aPDL1-SSL. a,d) Morphology and particle size distribution of CAR@aPDL1-SSL in PBS, b,e) CAR@aCD47/aPDL1-SSL in PBS, and c,f) in H_2O_2 determined by TEM and DLS (Scale bar: 100 nm). g,h) The immunofluorescence images of C6@aCD47/aPDL1-SSL and C6@aCD47-aPDL1-SSL in PBS and H_2O_2 , respectively (liposome [Coumarin-6 [C6], green], aPDL1 [Cy3, orange], aCD47 [Alexa Fluor647, red]) (Scale bar: 200 nm). i) The H_2O_2 scavenging efficiency of aCD47/aPDL1-SSL and aCD47-aPDL1-SSL. j) The release profiles of CAR encapsulated in SSL and aCD47/aPDL1-SSL.

respectively (Figure S2, Supporting Information). Compared with the zeta potential of sterically stabilized liposome (SSL), the zeta potential of aPDL1-SSL or aCD47-SSL was more negative (Figure S2, Supporting Information). The possible reason was the negatively charged aPDL1 or aCD47 that attached to the surface of the liposome. The zeta potential of aCD47/aPDL1-SSL was -40.78 ± 0.91 mV, and the electronegativity was significantly higher than the zeta potential of SSL possible because of the connection of multiple aPDL1 and aCD47 on the liposome surface (Figure S2, Supporting Information). This result also indicated that aPDL1 and aCD47 were successfully connected on the surface of aCD47/aPDL1-SSL. In addition, the zeta potential of CAR@aCD47/aPDL1-SSL was -39.12 ± 0.76 mV (Figure S2, Supporting Information). There was no significant difference observed in aCD47/aPDL1-SSL, indicating that the encapsulation of CAR did not affect the surface potential of liposomes. To further investigate the antibodies release sequence of aCD47/aPDL1-SSL, we first prepared a multifunctional immunoliposome (C6@aCD47/aPDL1-SSL) containing the green fluorescent probe coumarin-6 (C6) (Figure 2g,h). Consistent with the expectations, C6@aCD47/aPDL1-SSL responded to ROS and controlled the release of antibodies. In H₂O₂ solution, C6@aCD47/aPDL1-SSL released aCD47 (Alexa Fluor647, red) first, and then displayed aPDL1 (Cy3, orange) attached to the liposome surface (Figure 2h). But in PBS solution, the C6@aCD47/aPDL1-SSL did not release aCD47 (Figure 2g). Both aCD47 and aPDL1 were attached to the surface of liposomes (Figure 2g). The control immunoliposome (C6@aCD47-aPDL1-SSL), which contained ROS-stable linkers (bis-*N*-hydroxy succinimide [NHS]-modified pimelic acid), did not control the release of antibodies in response to ROS. It did not release aCD47 in either H₂O₂ solution or PBS solution (Figure 2g,h). In addition, the immunofluorescence colocalization of liposomes and antibodies also confirmed that aCD47 and aPDL1 were successfully linked on the surface of liposomes (Figure 2g). The ROS-sensitive linker on the liposome surface not only controlled the release sequence of antibodies, but also effectively scavenged ROS in the environment. The aCD47/aPDL1-SSL with ROS-sensitive linkers on the liposome surface significantly scavenged H₂O₂ compared with the control group aCD47-aPDL1-SSL, which contained ROS-stable linkers on the liposome surface (Figure 2i). The encapsulation efficiency (EE) of CAR was $52.8\% \pm 4.41\%$ and loading content (DL) was $16.23\% \pm 3.27\%$ determined by UV-spectrometer and HPLC. The conjugation efficiency rates of aCD47 and aPDL1 detected by the standard bicinchoninic acid (BCA) protein assay were 43% and 50%, respectively. The cumulative release rate of aCD47 from the multifunctional immunoliposome in H₂O₂ solution within 12 h was 98.7%. The CAR encapsulated in liposomes maintained a sustained release, and the cumulative release rate within 72 h was $\approx 68\%$ (Figure 2j). The tandem antibodies attached to the surface of the liposomes did not affect the release characteristics of CAR (Figure 2j). In H₂O₂ solution, the CAR encapsulated in liposomes also maintained a sustained release (Figure S3, Supporting Information). In addition, the cumulative release rate of CAR@aCD47/aPDL1-SSL in a PBS solution containing 10% FBS within 12 h was less than 10%, and the particle size of CAR@aCD47/aPDL1-SSL was ≈ 120 nm within 48 h, indicating that the multifunctional

immunoliposomes (CAR@aCD47/aPDL1-SSL) prepared in this research had good serum stability and ensured a high stability in physiological environment (Figure S4, Supporting Information).

2.2. The aCD47-Induced Immune Response

The CD47/SIRP α pathway (“do not eat me” pathway) has been considered to be an important mechanism by which tumor cells evade innate immune surveillance.^[17,18] However, innate immune cells, including macrophages and dendritic cells (DCs), play important roles in antigen presentation and T lymphocytes activation.^[37,38] In order to determine whether aCD47 can effectively block the “don’t eat me” pathway and whether it can promote the infiltration of tumor tissues by macrophages and DCs and activate T lymphocytes, we prepared aCD47-SSL and injected it into tumor-bearing mice intravenously. Compared with IgG-SSL, aCD47-SSL could significantly promote the infiltration of phagocytic cells, including macrophages and DCs into the tumor tissues (Figure 3a). Mature DCs play an important role in antigen presentation and T lymphocyte activation. Therefore, in order to further evaluate the effects of aCD47-SSL treatment, we further investigated the content of mature DCs in tumor tissues. After aCD47-SSL treatment, the mature DCs in tumor tissues including CD80⁺CD86⁺ DCs and CD103⁺ DCs increased significantly (Figure 3b,c). Furthermore, CD8⁺ T cells in tumor tissues increased significantly after aCD47-SSL treatment (Figure 3d,e). These results indicated that aCD47 can activate T cells by promoting the infiltration of phagocytes into tumor tissues and the maturation of DCs.

2.3. aCD47/aPDL1-SSL Scavenges Excessive Reactive Oxygen Species in Tumor Microenvironment

The immunosuppressive TME contains excessive ROS, which acts as signaling molecules and contribute to tumor growth, metastasis, and resistance to apoptosis.^[4–9,39] The ROS-sensitive linker (bis-*N*-hydroxy succinimide [NHS]-modified 2,2-[propane-2,2-diylbis (thio)] diacetic acid) synthesized in this study is composed of ROS-sensitive thioketal linkages.^[40] M.S. Shim et al. found that the high levels of ROS in cancer cells were exploited as a trigger mechanism, which led to the degradation of the thioketal linkages and to a controlled intracellular release of the encapsulated nucleic acids from the delivery agent.^[41] At the same time, the level of ROS in tumor tissues was downregulated due to the reaction with the thioketal linkages.^[41] To verify the ability of aCD47/aPDL1-SSL with ROS-sensitive linkers connected to its surface to scavenge ROS in TME, we investigated the changes in ROS level in TME and the immune response induced by the changes in ROS level. A control immunoliposome (aCD47-aPDL1-SSL) was also synthesized, in which ROS-sensitive linkers were substituted for ROS-stable linkers. We injected aCD47/aPDL1-SSL and aCD47-aPDL1-SSL intravenously into tumor-bearing mice every 3 days. And the ROS level in TME was observed at Day 21. As expected, the ROS level in TME significantly

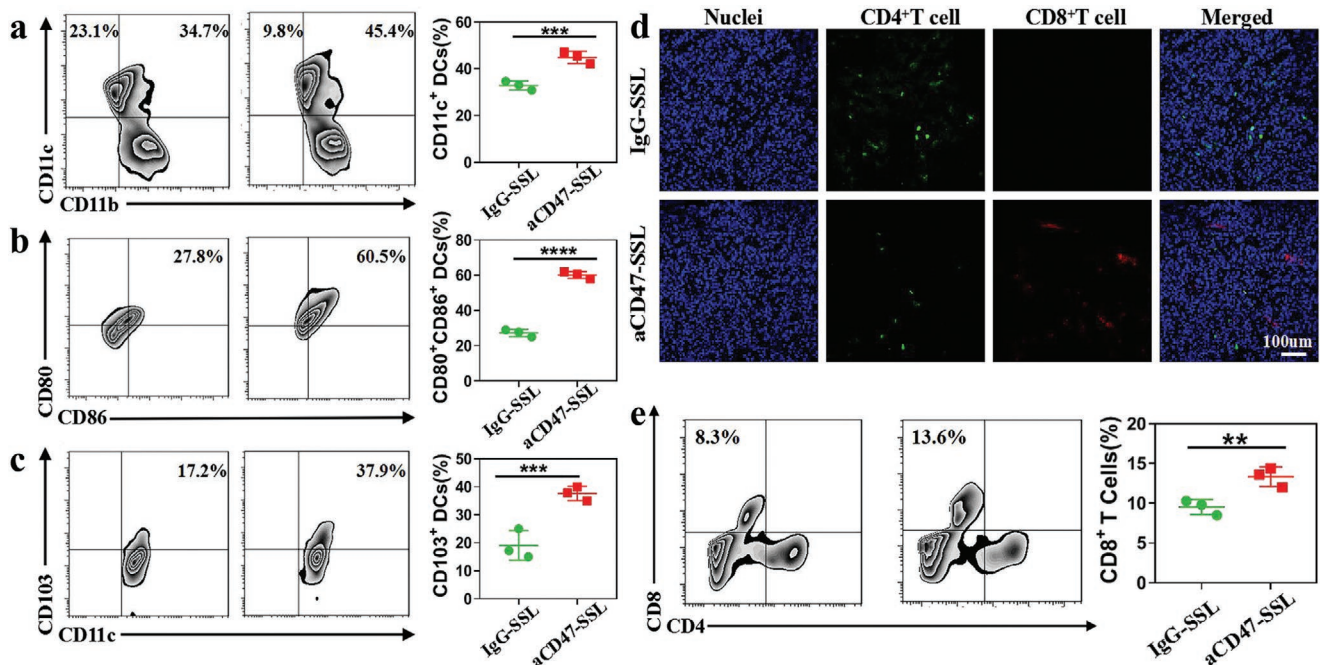


Figure 3. The aCD47-SSL promotes the infiltration of tumor tissues by macrophages and DCs and activates T lymphocytes. a) Flow cytometry detection and analysis of macrophages and CD11c⁺ DCs in tumor tissue after treatment of IgG-SSL and aCD47-SSL. b,c) Flow cytometry detection and analysis of CD80⁺CD86⁺ DCs and CD103⁺ DCs in tumor tissue. d,e) Immunofluorescence images and flow cytometry analysis of T cells in tumor after treatment of IgG-SSL and aCD47-SSL ($n = 3$, p value: * $p < 0.05$; ** $p < 0.01$; *** $p < 0.001$; **** $p < 0.0001$, Scale bar: 100 μm)

decreased after aCD47/aPDL1-SSL treatment compared with that after aCD47-aPDL1-SSL treatment (Figure 4a–d and Figure S5, Supporting Information). Studies highlighted the multiple roles of ROS and reactive nitrogen species in bystander effects.^[42,43] In addition, Wulf Dröge et al. found that free amino acids, peptides, and proteins can also act as ROS scavengers.^[44] The ROS-sensitive linkers on the surface of the multifunctional immunoliposome designed in our study can react with excess ROS in the tumor tissue, consume excess ROS in TME, and release aCD47. According to the study of Wulf Dröge et al., free aCD47 may play the role of ROS auxiliary scavenger and have a synergistic effect with ROS-sensitive linkers. Therefore, the low concentration of ROS-sensitive linkers in this study can effectively scavenge ROS in tumor tissues. To further determine the impact of decrease in ROS level in TME after aCD47/aPDL1-SSL treatment on immune system, we investigated the populations of different immune cells in tumor tissues including CD45⁺ cells, F4/80⁺CD206^{hi} M2 type tumor-associated macrophages (TAMs), CD3⁺CD4⁺Foxp3⁺regulatory T cells (Tregs), and CD8⁺ cytotoxic T cells (CTLs) (Figure 4e–j and Figure S6, Supporting Information). A significant reduction in M2-type TAMs and Tregs was observed in TME after aCD47/aPDL1-SSL treatment (Figure 4h,i). CTLs were significantly increased in the TME (Figure 4e,f,j and Figure S6, Supporting Information). Overall, the ROS-sensitive multifunctional immunoliposome aCD47/aPDL1-SSL scavenged ROS in TME, reduced the immunosuppressive cells, and promoted the infiltration of CTLs. Therefore, the effect of aPDL1 can be enhanced by reprogramming the immunosuppressive TME.

2.4. Blocking Adrenergic Nerve Fibers and Reprogramming the Immunosuppressive Tumor Microenvironment

The solid TME contains nerve fibers which arise from the peripheral nervous system.^[10,11] And the newly formed adrenergic nerve fibers can promote tumor angiogenesis, growth, and metastasis.^[10–12] Clinical data indicated that CAR, a blocker of β receptors, can prolong the survival of patients by inhibiting neoplastic adrenergic nerves.^[13,14] We hypothesized that CAR can have a synergistic effect with aPDL1 by blocking tumor adrenergic nerve fibers. To confirm this hypothesis, we first prepared a multifunctional immunoliposome encapsulating CAR, CAR@aCD47/aPDL1-SSL, and injected it intravenously into tumor-bearing mice. The common nerve markers MAP2 and NeuN were used in marking nerve fibers in tumor tissues, and the common blood vessel marker CD31 was used in marking blood vessels in tumor tissues. According to the results of immunofluorescence and immunohistochemistry, the density of nerve fibers in tumor tissues was significantly reduced after CAR@aCD47/aPDL1-SSL treatment, compared with PBS and aCD47/aPDL1-SSL group (Figure 5a–d and Figure S7a, Supporting Information). Then, we further investigated the effect of decreased nerve fiber density in tumor tissues. We found that after CAR@aCD47/aPDL1-SSL treatment, the blood vessel density in the tumor tissue also decreased significantly (Figure 5e–g and Figure S7b, Supporting Information). It might be that CAR blocked the adrenergic nerves in the tumor tissues and reduced their density, thereby inhibiting angiogenesis in the tumor tissues. In addition, compared with the PBS group, although the aCD47/aPDL1-SSL group did not

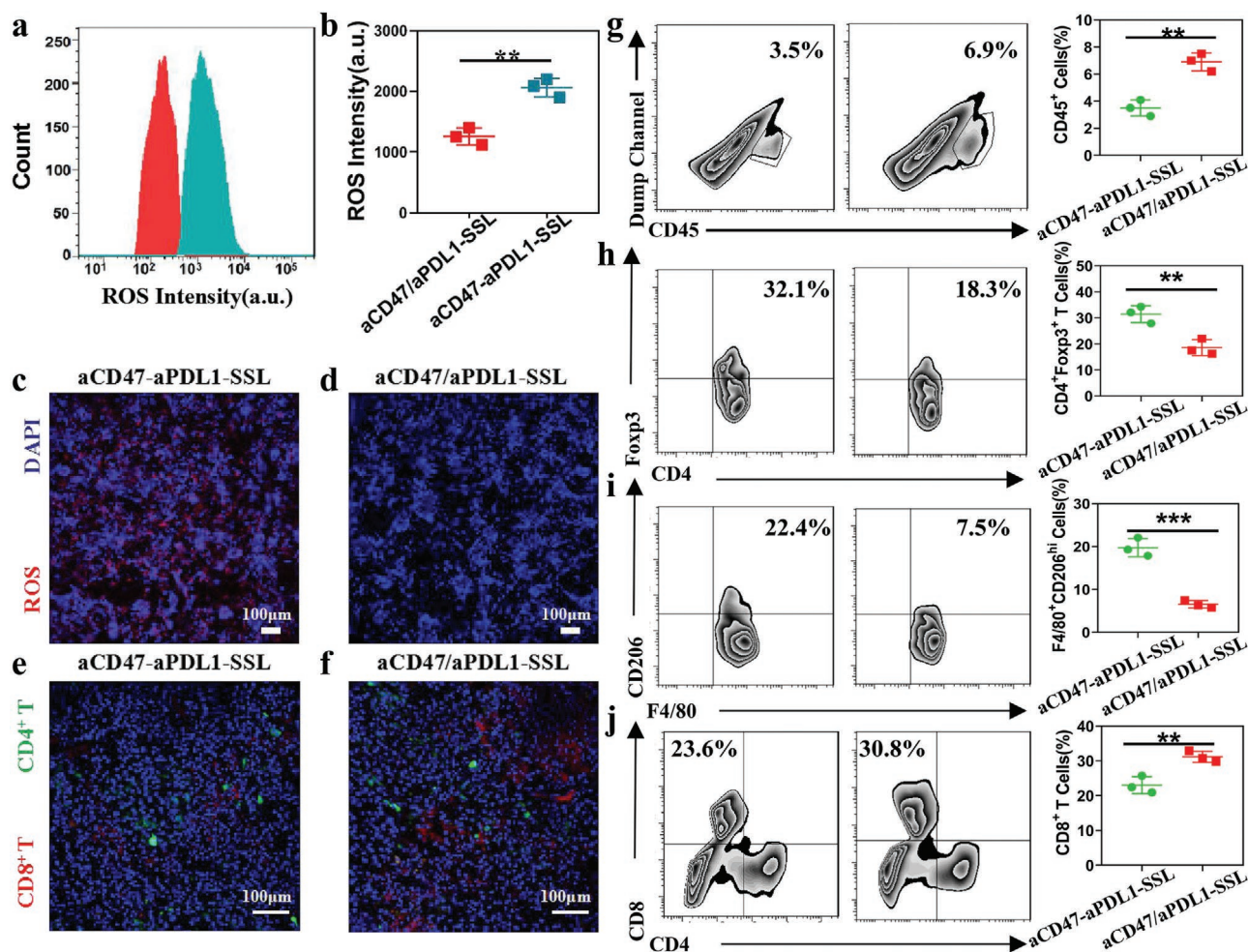


Figure 4. The ROS-sensitive immunoliposome aCD47/aPDL1-SSL scavenging ROS and reprogramming the immunosuppressive TME. a–d) Flow cytometry analysis and immunofluorescence images of ROS signal in TME after aCD47/aPDL1-SSL and aCD47-aPDL1-SSL treatment. g–j) Flow cytometry detection and analysis of CD45⁺ cells, F4/80⁺CD206^{hi} M2 type tumor-associated macrophages, and CD3⁺CD4⁺Foxp3⁺ regulatory T cells in tumor tissue. e, f, j) Immunofluorescence images and flow cytometry analysis of CD8⁺ cytotoxic T cells in tumor ($n = 3$, p value: * $p < 0.05$; ** $p < 0.01$; *** $p < 0.001$; **** $p < 0.0001$, Scale bar: 100 μm).

significantly reduce the density of the nerve fibers, it inhibited tumor angiogenesis (Figure 5e–g and Figure S7b, Supporting Information). This feature may be related to the ability of aCD47 to efficiently block the proliferation of vascular endothelial cells activated by NO and mediated by cGMP.^[45] Tumor angiogenesis is closely related to the tumor immunosuppressive microenvironment formation and tumor cell proliferation and metastasis.^[46,47] Therefore, we believe that CAR and aCD47, through indirect or direct processes that inhibit tumor angiogenesis, have a synergistic effect with aPDL1 to produce ideal antitumor effects.

2.5. Antitumor Efficacy and Safety of CAR@aCD47/aPDL1-SSL In Vivo

To demonstrate the antitumor efficiency of the multifunctional immunoliposomes in vivo, control (PBS), free aCD47/aPDL1, aPDL1-SSL, aCD47/aPDL1-SSL, and CAR@aCD47/aPDL1-SSL

were intravenously injected into B16-F10 tumor-bearing mice every 3 days ($\text{mol}_{\text{aCD47}}:\text{mol}_{\text{aPDL1}} = 1:1$, aPDL1: 1 mg kg⁻¹, CAR: 0.1 mg mL⁻¹) (Figure 6a). This results in CAR@aCD47/aPDL1-SSL showing an ideal antitumor effect. Compared with the other four groups, it significantly inhibited the growth of tumors and significantly prolonged the survival time of the tumor-bearing mice (Figure 6b–d). The antitumor effect of aCD47/aPDL1-SSL and CAR@aCD47/aPDL1-SSL was significantly higher than that of free aCD47/aPDL1, indicating that liposomes as nanocarriers enhanced the therapeutic effect of aCD47/aPDL1, likely due to the EPR effect. In addition, compared with aPDL1-SSL or aCD47/aPDL1-SSL, an obvious synergistic effect was achieved by CAR@aCD47/aPDL1-SSL. Furthermore, we investigated the infiltration of CD8⁺ T cells in tumor tissues after treatment with each group of formulations. According to the flow cytometry results, the population of CTLs in the tumor tissues significantly increased after the treatment of CAR@aCD47/aPDL1-SSL, compared with other four groups (Figure 6e, f). Immunofluorescence imaging also indicated that

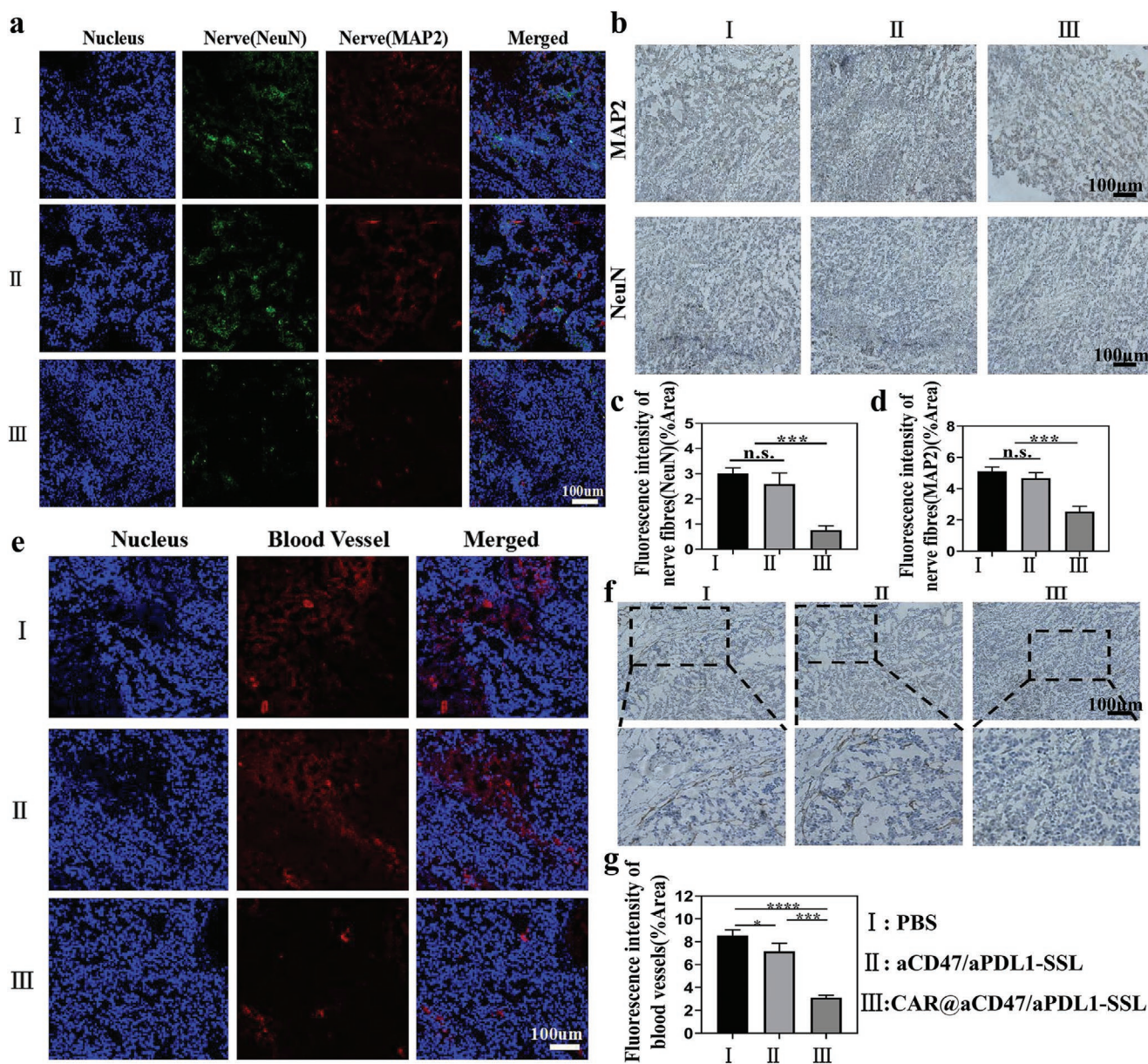


Figure 5. CAR@aCD47/aPDL1-SSL blocking adrenergic nerve fibers and inhibiting tumor angiogenesis. a–d) Immunofluorescence and immunohistochemistry images of adrenergic nerves (NeuN and MAP2) in TME after PBS, aCD47/aPDL1-SSL, and CAR@aCD47/aPDL1-SSL treatment. e–g) Immunofluorescence and immunohistochemistry images of tumor blood vessels (CD31) ($n = 3$, p value: $*p < 0.05$; $**p < 0.01$; $***p < 0.001$; $****p < 0.0001$, Scale bar: 100 μm).

there were more CTLs inflated into tumor tissue after CAR@aCD47/aPDL1-SSL treatment (Figure 6g and Figure S8a, Supporting Information). In addition, CAR@aCD47/aPDL1-SSL treatment could significantly promote tumor cell apoptosis, according to the results of H&E and TUNEL staining (Figure 6g and Figure S8b, Supporting Information). To further evaluate the antitumor immunity evoked by CAR@aCD47/aPDL1-SSL, we detected the cytokine production of tumor necrosis factor- α (TNF- α), interleukin-12 (IL-12), and interferon- γ (IFN- γ) in serum at Day 21. IFN- γ and TNF- α plays important roles in the antitumor immune response of cellular immunity. The IL-12 is the typical inflammatory cytokines and is a predictive factor

for the immune response. According to the results, the CAR@aCD47/aPDL1-SSL significantly promoted the release of inflammatory cytokines in serum, signifying that multifunctional immunoliposome studied in this research evoked inflammation and stimulated immune responses (Figure S9, Supporting Information).

The expression level of CD47 and PD-L1 in B16F10 cells were investigated after treatments. The results showed that the expression levels of CD47 and PD-L1 in B16F10 cells were significantly downregulated after CAR@aCD47/aPDL1-SSL treatment (Figure S10, Supporting Information). This result might be related to the reprogramming of the tumor

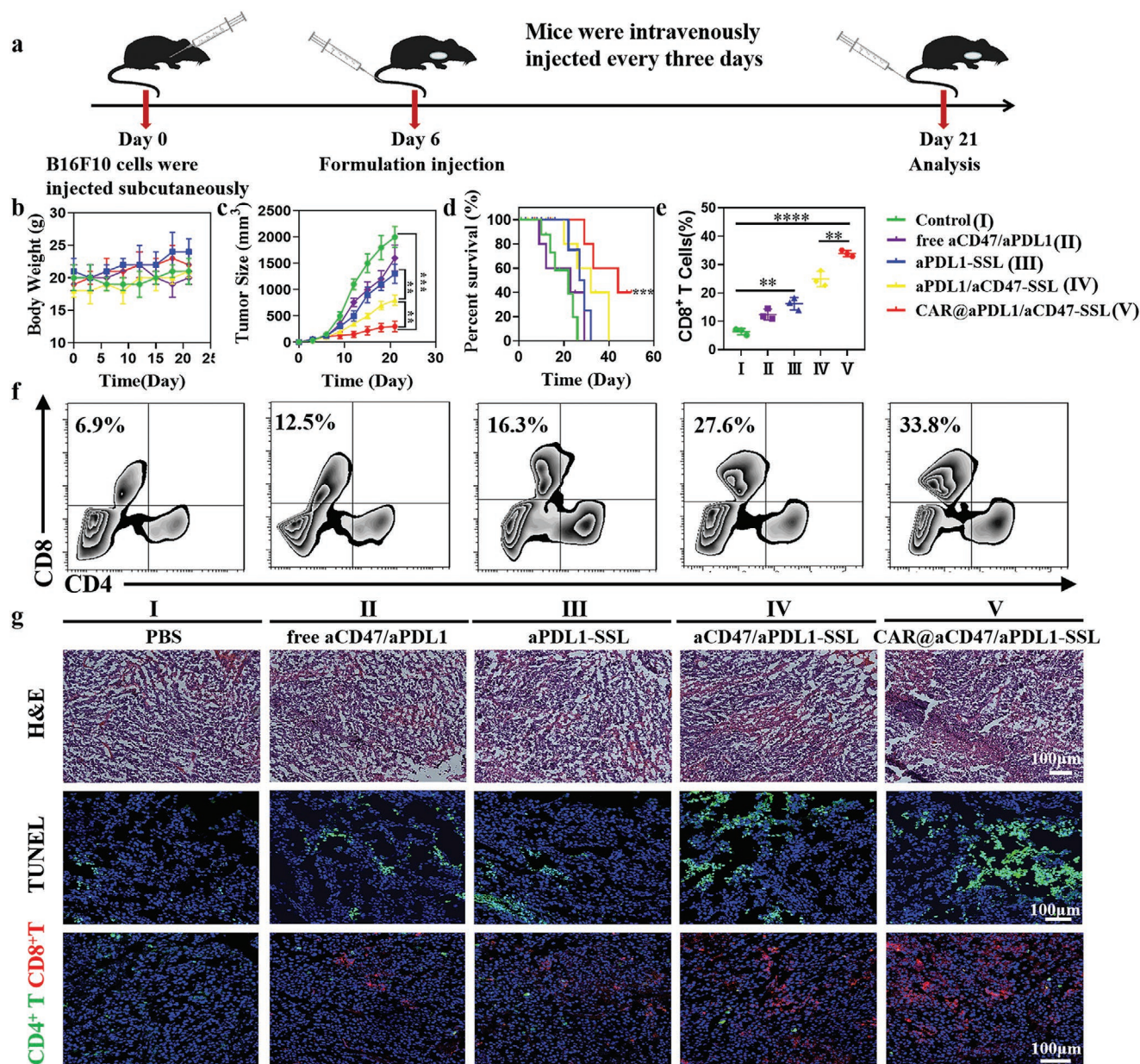


Figure 6. Antitumor efficacy of CAR@aCD47/aPDL1-SSL in vivo. a) Schematic illustration of tumor inoculation and the therapeutic schedule for CAR@aCD47/aPDL1-SSL-initiated antitumor study in vivo. b) The body weights of B16F10 tumor-bearing mice after treatment with PBS, aPDL1-SSLs, aCD47/aPDL1-SSL, and CAR@aCD47/aPDL1-SSL. c) The tumor volume of mice in each group. d) Survival curves of B16F10 tumor-bearing mice after treatment with each formulation described above. e, f) Flow cytometry detection and analysis of CD8⁺ cytotoxic T cells in tumor tissue after treatment with each formulation. g) Tumor cell apoptosis level detected by H&E and TUNEL staining and immunofluorescence images of CD8⁺ cytotoxic T cells in tumor after treated with each formulation ($n = 6$, p value: * $p < 0.05$; ** $p < 0.01$; *** $p < 0.001$; **** $p < 0.0001$, Scale bar: 100 μm).

immunosuppressive microenvironment after CAR@aCD47/aPDL1-SSL treatment. Immunosuppressive cells, including Treg,^[48] MDSCs,^[49,50] and TAM,^[51] could induce high PD-L1 and CD47 expression levels in tumor cells and inhibit the activation of CD8⁺ T cells, which gives the privilege to tumors for escaping the antitumor immunity.^[52–54] The above studies indicated that CAR@aCD47/aPDL1-SSL can reprogram the immunosuppressive TME, by suppressing immunosuppressive cells and activating CD8⁺ T cells. Therefore, CAR@aCD47/aPDL1-SSL

can significantly downregulate the expression levels of PD-L1 and CD47 by reprogramming the immunosuppressive TME, which is expected to enhance subsequent antitumor therapy. Collectively, these results indicated that the multifunctional immunoliposome, CAR@aCD47/aPDL1-SSL, can enhance the immune response mediated by CTLs, promote tumor cells apoptosis, and enhance the antitumor efficacy.

The safety of CAR@aCD47/aPDL1-SSL was investigated through H&E staining. According to the results, the morphology

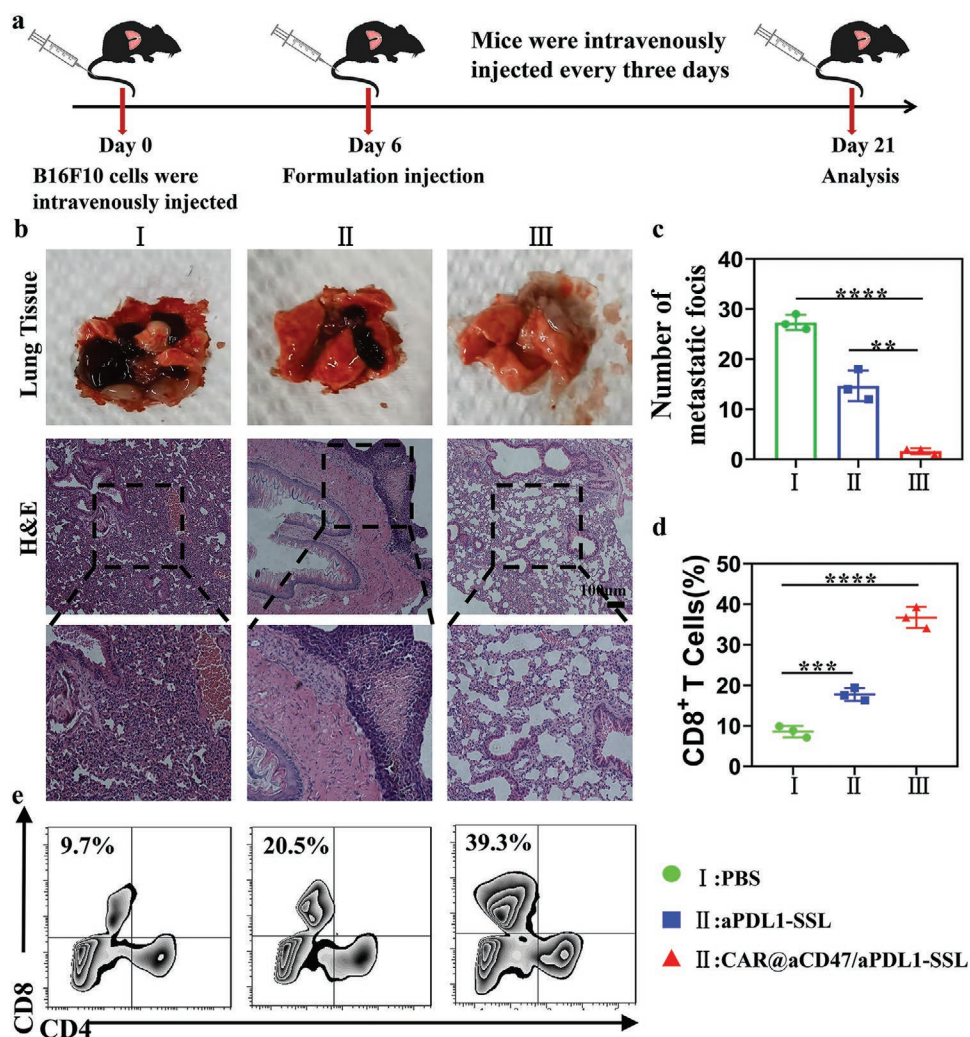


Figure 7. Suppression of lung tumor metastasis by CAR@aCD47/aPDL1-SSL. a) Schematic illustration for the suppression of tumor metastasis after intravenously injected PBS, aPDL1-SSL, and CAR@aCD47/aPDL1-SSL. b) The images and H&E staining results of the lung tissues after treatment with PBS, aPDL1-SSLs, and CAR@aCD47/aPDL1-SSL. c) Quantitative calculation of metastatic foci in lung tissues treated with different formulations. d,e) Flow cytometry detection and analysis of CD8⁺ cytotoxic T cells in blood of mice treated with each formulation ($n = 6$, p value: * $p < 0.05$; ** $p < 0.01$; *** $p < 0.001$; **** $p < 0.0001$, Scale bar: 100 μm).

of the heart, spleen, lungs, liver, and kidneys showed no obvious pathological abnormalities after different formulations treatments (Figure S11, Supporting Information). Accordingly, CAR@aCD47/aPDL1-SSL produced superior antitumor efficacy and did not produce systemic toxicity after continuous administration.

2.6. Suppression of Lung Tumor Metastasis by CAR@aCD47/aPDL1-SSL In Vivo

Tumor metastasis is considered one of the important causes of high tumor mortality.^[55] The above research results indicated that CAR@aCD47/aPDL1-SSL can simulate a powerful anti-tumor immune response mediated by CTLs. In order to further study its effect on the treatment of metastasis, we then constructed a B16F10 lung metastasis tumor model. Briefly, C57BL/6 mice were intravenously injected with B16F10 cells to

construct the lung metastasis tumor model, and the mice were treated with the PBS, aPDL1-SSL, and CAR@aCD47/aPDL1-SSL (Figure 7a). This results in the formation of lung metastasis being significantly suppressed after CAR@aCD47/aPDL1-SSL treatment, resulting in only 10.71% and 21.42% of the lung foci observed in PBS and aPDL1-SSL groups (Figure 7b,c). Furthermore, a lower degree of tumor invasion was observed in the lungs after CAR@aCD47/aPDL1-SSL treatment, whereas more observable damages were detected in aPDL1-SSL group in the H&E staining assay of the lung tissues (Figure 7b). This result indicated that an obvious synergistic effect was achieved by CAR@aCD47/aPDL1-SSL. In addition, a higher frequency of CTLs was detected in blood after treatment with CAR@aCD47/aPDL1-SSL (Figure 7d,e). Overall, these results indicated that CAR@aCD47/aPDL1-SSL can activate systemic immune response and suppress tumor metastasis, indicating a better antitumor therapeutic effect.

3. Conclusion

In conclusion, we have successfully developed a multifunctional immunoliposome (CAR@aCD47/aPDL1-SSL) encapsulating an adrenergic receptor blocker CAR, and connecting aCD47 and aPDL1 in series via a ROS-sensitive linker on the surface. This multifunctional immunoliposome possesses several advantages: 1) the antibodies attached to the surface of liposomes can be released sequentially in response to ROS signals in TME, resulting in a synergistic effect. In ROS-enriched immunosuppressive TME, the multifunctional immunoliposome (CAR@aCD47/aPDL1-SSL) can first release the outer aCD47 to block the “do not eat me” pathway, promote the phagocytosis of tumor cells by phagocytic cells and activate T lymphocytes. Then the aPDL1 on the liposome surface is exposed to block the PD-1/PD-L1 signaling pathway, thereby promoting T lymphocytes to recognize tumor cells and kill tumor cells. 2) The multifunctional immunoliposome could reprogram the immunosuppressive TME and promote the infiltration of CTLs in tumors. ROS-sensitive linkers on the surface of the CAR@aCD47/aPDL1-SSL can not only control the sequential release of antibodies on the liposome surface, but also scavenge ROS in the TME, thereby reducing M2-type TAMs and Tregs and increasing CTLs in TME. CAR encapsulated in CAR@aCD47/aPDL1-SSL can block the adrenergic nerves in the tumor tissues and reduce their density, thereby inhibiting angiogenesis in the tumor tissues and reprogramming the immunosuppressive TME. 3) CAR@aCD47/aPDL1-SSL can enhance the immune response mediated by CTLs, promote tumor cells apoptosis, and enhance the antitumor efficacy. Furthermore, CAR@aCD47/aPDL1-SSL can induce systemic immune response and effectively inhibit cancer metastasis. Therefore, this multifunctional immunoliposome established an effective strategy for delivering antibodies and reprogramming the immunosuppressive TME, providing a potential way for significantly enhancing immunotherapeutic efficiency against the primary cancer and metastasis.

4. Experimental Section

Materials: The Lecithin (soy beans) (SPC), cholesterol, 2,2'-[propane-2,2-diylbis-(thio)] diacetic acid, pimelic acid, 1-ethyl-3-(3-(dimethylamino) propyl)-carbodiimide (EDC), and *N*-hydroxy-succinimide (NHS) were all purchased from Sigma Aldrich (St. Louis, USA). C6 was purchased from Aladdin Bio-Chem Technology Co. Ltd (Shanghai, China). DSPE-PEG2000 (distearoylphosphatidylethanolamine-methoxy-polyethylene glycol) and DSPE-PEG2000-NHS (1,2-distearoyl-*sn*-glycero-3-phosphoethanolamine-*N*-[succinimidyl (polyethylene glycol)]) were purchased from Corden Pharm (Eichenweg, Switzerland). aCD47 (Clone: miap301) and antibody of PDL1 (aPDL1) (Clone: 10F.9G2) were both purchased from Bio X Cell (West Lebanon, NH, USA).

Cell Lines and Animals: The melanoma cell line of mouse (B16F10) was purchased from Cell Resource Center, Chinese Academy of Medical Sciences. The B16F10 cells were cultured at 37 °C in 5% CO₂ in Dulbecco's modified eagle medium (Gibco, Invitrogen, USA) supplemented with 100 U mL⁻¹ penicillin (Invitrogen, USA), 100 U mL⁻¹ streptomycin (Invitrogen, USA), and 10% fetal bovine serum (Invitrogen, USA). The age-matched (6–8 weeks) female C57BL/6 mice were purchased from Beijing Vital River Laboratory Animal Technology Co., Ltd (Beijing, China). In addition, animal experiments in this research were conducted following the animal protocols approved by the Ethics

Committee on Laboratory Animal Welfare of Peking University. And the assigned approval number of the laboratory in the Experimental Section of this manuscript was LA2019197.

Preparation of CAR@aCD47/aPDL1-SSL: The synthesis and detection of DSPE-PEG2000-aPDL1 and preparation of basic SSLs and aPDL1-SSL were consistent with those reported in previous studies.^[36] aCD47-SSL was also prepared by the film dispersion/postinsertion method, which was the same as the preparation method of aPDL1-SSL. First, DSPE-PEG2000-NHS was mixed with aCD47 (Clone: miap301) (Bio X Cell, West Lebanon, NH, USA) at a molar ratio of 10:1 to form the leading compound, DSPE-PEG2000-aCD47. Then DSPE-PEG2000-aCD47 was incubated with SSL at a ratio of 1:100 for 4 h with continuous stirring to form aCD47-SSLs. Excessive aCD47s were removed using a dialysis membrane with a 300-kDa molecular weight cut off (MWCO) (Mmbio, China). To prepare multifunctional immunoliposome CAR@aCD47/aPDL1-SSL, the authors first synthesized the ROS-sensitive linker. 2,2'-[propane-2,2-diylbis (thio)] diacetic acid, EDC, and NHS were dissolved in 2 mL dimethyl sulfoxide at a molar ratio of 1:2:2 and stirred for 6 h at room temperature. And then the synthesized ROS-sensitive linker (bis-*N*-hydroxy succinimide [NHS]-modified 2,2'-[propane-2,2-diylbis (thio)] diacetic acid) was detected by mass spectrometry (Solarix XR, Bruker, Germany). The ROS-stable linker (bis-*N*-hydroxy succinimide [NHS]-modified pimelic acid) was synthesized using the same method with pimelic acid as raw material. To prepare CAR@SSL, SPC, cholesterol, and DSPE-PEG2000 were dissolved in 1 mL of chloroform at a molar ratio of 100:50:8. Then CAR was also added to the chloroform. Next, the dried lipid was hydrated using 2 mL PBS solution. DSPE-PEG2000-aPDL1 was then incubated with CAR@SSL at a ratio of 1:100 for 4 h with continuous stirring to form CAR@aPDL1-SSL. The ROS-sensitive linker, aCD47 and CAR@aPDL1-SSL were incubated for 12 h at 4 °C with continuous stirring to form CAR@aCD47/aPDL1-SSL. The molar ratio of aPDL1 to aCD47 was 1:1 and concentration of CAR was 0.1 mg mL⁻¹. Excessive aPDL1 and aCD47 were removed using a dialysis membrane with 300 kDa MWCO (Mmbio, China).^[36] Excessive CAR was removed using a dialysis membrane with 3500 Da MWCO and the external dialysis fluid was acetic acid solution (0.06 mol L⁻¹). C6-loaded immunoliposomes (C6@aCD47/aPDL1-SSLs) and CAR@aCD47-aPDL1-SSL, in which ROS-stable linker was substituted for ROS-sensitive linker, were also prepared using the film dispersion method mentioned above.

Characterization of CAR@aCD47/aPDL1-SSL: The particle size, polydispersity, and zeta potential of CAR@aCD47/aPDL1-SSL were measured using DLS (Zetasizer Nano ZS90, Malvern, United Kingdom). And TEM (JEM-1400Plus, JEOL, Tokyo, Japan) was used to observe the morphology of CAR@aCD47/aPDL1-SSL after the sample was stained with 2% w/v phosphotungstic acid solution. The EE, loading content (DL), and cumulative release rate of CAR was measured using the UV spectrophotometer (UV3600PLUS, Shimadzu, Japan) and HPLC (Shimadzu, Japan) at 331 nm wavelength. The HPLC analysis was conducted on a Shimadzu LC-20A system (Shimadzu, Japan) equipped with a Thermo C18 column (5 μm, 4.6 × 250 mm) and UV-vis detector using methanol/PBS/glacial acetic acid (6:4:0.3 volume ratio) as an eluent. The flow rate was 1.0 mL min⁻¹. EE% was calculated using formula consistent with previous studies.^[36] DL% was calculated using the following formula:

$$DL(\%) = \frac{\text{Weight of the CAR in liposome}}{\text{Weight of liposome}} \times 100\% \quad (1)$$

The conjugation efficiency of aCD47 or aPDL1 was determined by the standard BCA protein assay (Solarbio Science & Technology Co., Ltd, China). The optical density value of each well was measured by a microplate reader with a wavelength of 570 nm.

The in vitro release behavior of CAR from CAR@SSL and CAR@aCD47/aPDL1-SSL was investigated using dialysis diffusion method. Briefly, 2 mL of CAR@SSL or CAR@aCD47/aPDL1-SSL solution was added into each dialysis bag (MWCO 3500 Da). Then, the dialysis bags were kept in 10 mL release medium (PBS solution and H₂O₂ solution)

at 37 ± 0.5 °C with horizontal shaking (100 rpm). At predetermined time intervals, 1 mL of the release medium outside the dialysis bag was took out and replaced with isometric fresh medium, and the content of CAR in harvest sample was detected by the UV spectrophotometer (UV3600PLUS, Shimadzu, Japan) and HPLC (Shimadzu, Japan) at 331 nm wavelength. The stability of CAR@aCD47/aPDL1-SSL in serum was also investigated by dialysis diffusion method. The cumulative release rate of aCD47 from the multifunctional immunoliposome in H₂O₂ solution with 12 h was also investigated using dialysis diffusion method. The basic operation was the same as above. The fluorescence-labeled aCD47 (Alexa Fluor647, red) was also purchased from Bio X Cell (West Lebanon, NH, USA; Clone: 10F.9G2). The MWCO of the dialysis bag was 300-kDa (Mmbio, China). The content of aCD47 in harvest sample was detected by fluorescence spectrometer (F7000, HITACHI, Japan).

The H₂O₂ scavenging rate of aCD47-aPDL1-SSL and aCD47/aPDL1-SSL were measured using the UV spectrophotometer at 230 nm wavelength and were calculated according to the following formula:

$$\text{H}_2\text{O}_2 \text{ scavenging rate (100\%)} = \left[1 - \frac{(A_s - A_b)}{A_c} \right] \times 100\% \quad (2)$$

where A_s was defined as the absorbance of H₂O₂ remaining after adding the sample, A_b was defined as the absorbance of sample, and A_c was defined as the absorbance of H₂O₂ remaining after adding after adding vitamin C.

C6@aCD47/aPDL1-SSL, fluorescence-labeled aCD47 antibodies, and aPDL1 antibodies (Abcam, Cambridge, UK) were used to confirm that aPDL1 and aCD47 were successfully attached to the surface of the liposomes in series via a ROS-sensitive linker and had ROS-responsive release characteristics. C6@aCD47-aPDL1-SSL was used as a control, in which ROS-sensitive linkers were substituted for ROS-stable linkers. C6@aCD47/aPDL1-SSL and C6@aCD47-aPDL1-SSL were incubated in H₂O₂ and PBS (pH 7.4) for 2 h at room temperature and then observed using confocal laser scanning microscopy (CLSM) (A1Rsi, Nikon, Tokyo, Japan).

Reactive Oxygen Species Levels in Tumor Microenvironment: In order to detect the ROS levels in TME after treated with aCD47/aPDL1-SSL, the authors first built tumor-bearing animal model. C57BL/6 (6–8 weeks of age, 20 g b⁻¹) mice were injected with B16F10 cells subcutaneously in the right flank at a density of 1×10^6 . When the tumor volume reached 100 mm³, the tumor-bearing mice were divided into two groups. They were then intravenously injected with aCD47/aPDL1-SSL and aCD47-aPDL1-SSL (control group) ($\text{mol}_{\text{aCD47}}:\text{mol}_{\text{aPDL1}} = 1:1$, aPDL1: 1 mg kg⁻¹). ROS levels in the tumor tissue collected from mice treated with aCD47/aPDL1-SSL or aCD47-aPDL1-SSL were detected via the CellROX deep red reagent (Invitrogen, USA) by flow cytometry (FACSCalibur, BD Biosciences, San Jose, CA, USA) and CLSM (A1Rsi, Nikon, Tokyo, Japan).

Infiltration of Immune Cells in Tumor Tissue: To investigate infiltration of different immune cells in the tumor tissue, tumors collected from mice after treatment with different formulations were cut into small pieces and homogenized to form single cells in cold staining buffer. Immune cells were stained with fluorescence-labeled antibodies CD45 (clone: 30-F11), CD11c (clone: N418), CD11b (clone: M1/70), CD80 (clone: 16-10A1), CD86 (clone: GL-1), CD103 (clone: 2E7), Foxp3 (clone: MF-14), CD206 (clone: C068C2), F4/80 (clone: BM8), CD3 (clone: 17A2), CD4 (clone: GK1.5), and CD8 (clone: 53-6.7) following the manufactures' instructions. All the fluorescence-labeled antibodies were purchased from Biologend company (California, USA). Antibodies used here were diluted 200 times. Then stained immune cells were detected by flow cytometry (FACSCalibur, BD Biosciences, San Jose, CA, USA) and analyzed by FlowJo software (version 10.0.7). Further, infiltration of CTLs in tumor tissue were observed using CLSM. 4',6-diamidino-2-phenylindole (DAPI) (Solarbio, China) was used to label the nucleus of B16F10 cells, and fluorescence-labeled CD4⁺ and CD8⁺ antibodies were used to label the T lymphocytes in tumor tissue (Biologend, USA). The results of immunofluorescence staining were observed using CLSM (Nikon, A1R-si, Japan).

Adrenergic Nerve Fibers and Blood Vessels in Tumor Microenvironment: To investigate adrenergic nerve fibers and blood vessels in the tumor tissue, tumors were collected from mice after treatment with different formulations and frozen in optimal cutting temperature medium. Then tumors were cut via a cryotome and mounted on slides. DAPI (Solarbio, China) was used to label the nucleus of B16F10 cells. Antibodies NeuN (Bioss, China) and MAP2 (Bioss, China) were used to label the adrenergic nerves and CD31 (Invitrogen, USA) was used to label the blood vessels in tumor. The results were observed by immunofluorescence staining and immunohistochemical analysis. The quantitative analysis of the results was analyzed by ImageJ software (version 1.8.0).

Antitumor Efficacy and Safety Study In Vivo: To evaluate the antitumor efficacy of immunoliposomes, the tumor-bearing mice were randomly divided into four groups ($n = 6$) and intravenously injected with PBS, free aCD47/aPDL1, aPDL1-SSL, aCD47/aPDL1-SSL, CAR@aCD47/aPDL1-SSL ($\text{mol}_{\text{aCD47}}:\text{mol}_{\text{aPDL1}} = 1:1$, aPDL1: 1 mg kg⁻¹, CAR: 0.1 mg mL⁻¹) every 3 days. During the treatment period, the weight of the mice and the volume of tumors were recorded to evaluate the antitumor efficacy of each formulations. The tumor volumes were calculated by the formula: Volume = length \times width²/2. The survival curve of tumor-bearing mice was analyzed using GraphPad Prism software (version 8.0.1). After treatment with different formulations, the infiltration of CTLs in tumor tissues of the mice was investigated by the same method mentioned above using flow cytometry and CLSM. The apoptosis of tumor cells after treated with different formulations was investigated by H&E staining and TUNEL assay kit (Solarbio, China). The cytokines in serum including TNF- α (4A Biotech Co., Ltd), IL12 (4A Biotech Co., Ltd), and IFN- γ (4A Biotech Co., Ltd) were detected by enzyme-linked immunosorbent assay according to the protocol. The CD47 and PD-L1 expression level in B16F10 cells was detected by flow cytometer assay. Finally, to evaluate the safety of using immunoliposomes in vivo, the main organs of mice were collected for H&E staining.

Suppression of Lung Tumor Metastasis by CAR@aCD47/aPDL1-SSL In Vivo: To evaluate the suppression effect of CAR@aCD47/aPDL1-SSL on metastasis, the authors first built the lung metastatic model of B16F10 cells. C57BL/6 (6–8 weeks of age, 20 g b⁻¹) mice were injected with B16F10 cells intravenously at a density of 1×10^5 . At 6 day post injection of cells, the tumor-bearing mice were divided into three groups ($n = 6$). They were then intravenously injected with PBS, aPDL1-SSL, and CAR@aCD47/aPDL1-SSL ($\text{mol}_{\text{aCD47}}:\text{mol}_{\text{aPDL1}} = 1:1$, aPDL1: 1 mg kg⁻¹) every 3 days. On Day 21, the mice were sacrificed, and the lung tissues were collected. Then the metastatic lung tumor lesions were photographed and counted visually. Furthermore, the lung tissues were observed by H&E staining for assessing the metastatic area. In addition, after treatment with different formulations, the CTLs in blood of the mice were also investigated by the same method mentioned above using flow cytometry.

Statistical Analysis: The data were presented as the means \pm SD. Mean values were compared using the two-tailed Student's *t*-test. $p < 0.05$ (*), $p < 0.01$ (**), $p < 0.001$ (***) and $p < 0.0001$ (****) were considered statistically significant.

Supporting Information

Supporting Information is available from the Wiley Online Library or from the author.

Acknowledgements

This work was afforded by the National Natural Science Foundation of China (No. 81571824), Peking University's 985 grant, National Key Research and Development Program of China (2016YFC0906000, 2016YFC0906001), the Ministry of Science and Technology (MOST) of China for the program (2020YFC0848700), and the Qidong-SLS Innovation Fund (to X.D.S.). The authors thank the National Center for

Protein Science at Peking University in Beijing, China, for assistance with instruction of using flow cytometer. The authors acknowledge Prof. Jingwei Xiong, Prof. Yixiang Wang, and Prof. Jianyong Huang for their guidance and help.

Conflict of Interest

The authors declare no conflict of interest.

Author Contributions

The manuscript was written through contributions of all authors. All authors have given approval to the final version of the manuscript.

Data Availability Statement

Research data are not shared.

Keywords

“don't eat me” signal antibody (aCD47), adrenergic nerve fibers, immunosuppressive tumor microenvironment, multifunctional immunoliposomes, PD-L1 antibody (aPDL1)

Received: August 25, 2021

Revised: November 24, 2021

Published online:

- [1] H. Phuengkham, L. Ren, I. W. Shin, Y. T. Lim, *Adv. Mater.* **2019**, *31*, 1803322.
- [2] Z. Yang, D. Gao, X. Q. Guo, L. Jin, J. J. Zheng, Y. Wang, S. J. Chen, X. W. Zheng, L. Zeng, M. Guo, X. C. Zhang, Z. M. Tian, *ACS Nano* **2020**, *14*, 17442.
- [3] M. J. Smyth, S. F. Ngiew, A. Ribas, M. W. L. Teng, *Nat. Rev. Clin. Oncol.* **2016**, *13*, 143.
- [4] C. Wang, J. Q. Wang, X. D. Zhang, S. J. Yu, D. Wen, Q. Y. Hu, Y. Q. Ye, H. Bomba, X. L. Hu, Z. Liu, G. P. Dotti, Z. Gu, *Sci. Transl. Med.* **2018**, *10*, eaan3682.
- [5] S. J. Yu, C. Wang, J. C. Yu, J. J. Wang, Y. Lu, Y. Q. Zhang, X. D. Zhang, Q. Y. Hu, W. J. Sun, C. L. He, X. S. Chen, Z. Gu, *Adv. Mater.* **2018**, *30*, 1801527.
- [6] C. Nathan, A. Cunningham-Bussel, *Nat. Rev. Immunol.* **2013**, *13*, 349.
- [7] N. S. Katheder, R. Khezri, F. O'Farrell, S. W. Schultz, A. Jain, M. M. Rahman, K. O. Schink, T. A. Theodossiou, T. Johansen, G. Juhász, D. Bilder, A. Brech, H. Stenmark, T. E. Rusten, *Nature* **2017**, *541*, 417.
- [8] S. S. Sabharwal, P. T. Schumacker, *Nat. Rev. Cancer* **2014**, *14*, 709.
- [9] J. N. Moloney, J. Stanicka, T. G. Cotter, *Leuk. Res.* **2017**, *52*, 34.
- [10] C. Magnon, S. J. Hall, J. Lin, X. N. Xue, L. Gerber, S. J. Freedland, P. S. Frenette, *Science* **2013**, *341*, 1236361.
- [11] G. E. Ayala, H. Dai, M. Powell, R. Li, Y. Ding, T. M. Wheeler, D. Shine, D. Kadmon, T. Thompson, B. J. Miles, M. M. Ittmann, D. Rowley, *Clin. Cancer Res.* **2008**, *14*, 7593.
- [12] A. H. Zahalka, A. Arnal-Estapé, M. Maryanovich, F. Nakahara, C. D. Cruz, L. W. S. Finley, P. S. Frenette, *Science* **2017**, *358*, 321.
- [13] A. Melhem-Bertrandt, M. Chavez-MacGregor, X. D. Lei, E. N. Brown, R. T. Lee, F. Meric-Bernstam, A. K. Sood, S. D. Conzen, G. N. Hortobagyi, A. M. Gonzalez-Angulo, *J. Clin. Oncol.* **2011**, *29*, 2645.
- [14] C. S. Lin, W. S. Lin, C. L. Lin, C. H. Kao, *Int. J. Cardiol.* **2015**, *184*, 9.
- [15] J. T. Sockolosky, M. Dougan, J. R. Ingram, C. C. M. Ho, M. J. Kauke, S. C. Almo, H. L. Ploegh, K. C. Garcia, *Proc. Natl. Acad. Sci. USA* **2016**, *113*, E2646.
- [16] S. B. Willingham, J. P. Volkmer, A. J. Gentles, D. Sahoo, P. Dalerba, S. S. Mitra, J. Wang, H. Contreras-Trujillo, R. Martin, J. D. Cohen, P. Lovelace, F. A. Scheeren, M. P. Chao, K. Weiskopf, C. Tang, A. K. Volkmer, T. J. Naik, T. A. Storm, A. R. Mosley, B. Edris, S. M. Schmid, C. K. Sun, M. S. Chua, O. Murillo, P. Rajendran, A. C. Cha, R. K. Chin, D. Kim, M. Adorno, T. Raveh, et al., *Proc. Natl. Acad. Sci. USA* **2012**, *109*, 6662.
- [17] R. Majeti, M. P. Chao, A. A. Alizadeh, W. W. Pang, S. Jaiswal, K. D. G. Jr, N. van Rooijen, I. L. Weissman, *Cell* **2009**, *138*, 286.
- [18] S. Jaiswal, C. H. M. Jamieson, W. W. Pang, C. Y. Park, M. P. Chao, R. Majeti, D. Traver, N. v. R., I. L. Weissman, *Cell* **2009**, *138*, 271.
- [19] M. P. Chao, A. A. Alizadeh, C. Tang, J. H. Myklebust, B. Varghese, S. Gill, M. Jan, A. C. Cha, C. K. Chan, B. T. Tan, C. Y. Park, F. Zhao, H. E. Kohrt, R. Malumbres, J. Briones, R. D. Gascoyne, I. S. Lossos, R. Levy, I. L. Weissman, R. Majeti, *Cell* **2010**, *142*, 699.
- [20] Y. T. Huang, Y. C. Ma, P. Gao, Z. Yao, *J. Thorac. Dis.* **2017**, *9*, E168.
- [21] S. Subramanian, R. Parthasarathy, S. Sen, E. T. Boder, D. E. Discher, *Blood* **2006**, *107*, 2548.
- [22] R. H. Vonderheide, *Nat. Med.* **2015**, *21*, 1122.
- [23] D. Mittal, M. M. Gubin, R. D. Schreiber, M. J. Smyth, *Curr. Opin. Immunol.* **2014**, *27*, 16.
- [24] S. R. Gordon, R. L. Maute, B. W. Dulken, G. Hutter, B. M. George, M. N. McCracken, R. Gupta, J. M. Tsai, R. Sinha, D. Corey, A. M. Ring, A. J. Connolly, I. L. Weissman, *Nature* **2017**, *545*, 495.
- [25] H. Tao, P. D. Qian, F. J. Wang, H. L. Yu, Y. S. Guo, *Oncol. Res.* **2017**, *25*, 1579.
- [26] Q. Chen, C. Wang, X. D. Z., G. J. Chen, Q. Y. Hu, H. J. Li, J. Q. Wang, D. Wen, Y. Q. Zhang, Y. F. Lu, G. Yang, C. Jiang, J. Wang, G. Dotti, Z. Gu, *Nat. Nanotechnol.* **2019**, *14*, 89.
- [27] A. J. Minn, E. J. Wherry, *Cell* **2016**, *165*, 272.
- [28] T. F. Gajewski, H. Schreiber, Y. X. Fu, *Nat. Immunol.* **2013**, *14*, 1014.
- [29] M. Leisegang, T. Kammertoens, W. Uckert, T. Blankenstein, *J. Clin. Invest.* **2016**, *126*, 854.
- [30] Z. Eroglu, J. M. Zaretsky, S. Hu-Lieskovan, D. W. Kim, A. Algazi, D. B. Johnson, E. Liniker, B. Kong, R. Munhoz, S. Rapisuwon, P. F. Gherardini, B. Chmielowski, X. Y. Wang, I. P. Shintaku, C. Wei, J. A. Sosman, R. W. Joseph, M. A. Postow, M. S. Carlino, W. J. Hwu, R. A. Scolyer, J. Messina, A. J. Cochran, G. V. L., A. Ribas, *Nature* **2018**, *553*, 347.
- [31] A. Ribas, J. D. Wolchok, *Science* **2018**, *359*, 1350.
- [32] J. Naidoo, D. B. Page, B. T. Li, L. C. Connell, K. Schindler, M. E. Lacouture, M. A. Postow, J. D. Wolchok, *Ann. Oncol.* **2015**, *26*, 2375.
- [33] M. Mellati, K. D. Eaton, B. M. Brooks-Worrell, W. A. Hagopian, R. Martins, J. P. Palmer, I. B. Hirsch, *Diabetes Care* **2015**, *38*, e137.
- [34] B. Felice, M. P. Prabhakaran, A. P. Rodríguez, S. Ramakrishna, *Mater. Sci. Eng., C* **2014**, *41*, 178.
- [35] H. Kobayashi, R. Watanabe, P. L. Choyke, *Theranostics* **2014**, *4*, 81.
- [36] Y. Hei, B. H. Teng, Z. Q. Zeng, S. Q. Zhang, Q. Li, J. J. Pan, Z. Y. Luo, C. Y. Xiong, S. C. Wei, *Int. J. Nanomed.* **2020**, *15*, 1677.
- [37] B. Edris, K. Weiskopf, A. K. Volkmer, J. P. Volkmer, S. B. Willingham, H. Contreras-Trujillo, J. Liu, R. Majeti, R. B. West, J. A. Fletcher, A. H. Beck, I. L. Weissman, M. van de Rijn, *Proc. Natl. Acad. Sci. USA* **2012**, *109*, 6656.
- [38] A. D. Michaels, T. E. Newhook, S. J. Adair, S. Morioka, B. J. Goudreau, S. Nagdas, M. G. Mullen, J. B. Persily,

- T. N. J. Bullock, C. L. S. Jr, K. S. Ravichandran, J. T. Parsons, T. W. Bauer, *Clin. Cancer Res.* **2018**, *24*, 1415.
- [39] H. D. Tang, Y. Wang, L. K. Chlewicki, Y. Zhang, J. Y. Guo, W. Liang, J. Y. Wang, X. X. Wang, Y. X. Fu, *Cancer Cell* **2016**, *30*, 500.
- [40] D. S. Wilson, G. Dalmaso, L. X. Wang, S. V. Sitaraman, D. Merlin, N. Murthy, *Nat. Mater.* **2010**, *9*, 923.
- [41] M. S. Shim, Y. N. Xia, *Angew. Chem., Int. Ed.* **2013**, *52*, 6926.
- [42] J. P. Pouget, A. G. Georgakilas, J. L. Ravanat, *Antioxid. Redox Signaling* **2018**, *20*, 1447.
- [43] H. Shao, H. Y. Y. Cheng, R. G. Cook, D. J. Tweardy, *Cancer Res.* **2003**, *15*, 3923.
- [44] W. Dröge, *Physiol. Rev.* **2002**, *82*, 47.
- [45] E. Sick, A. Jeanne, C. Schneider, S. Dedieu, K. Takeda, L. Martiny, *Br. J. Pharmacol.* **2012**, *167*, 1415.
- [46] A. Canoğlu, C. Göğüş, Y. Bedük, D. Orhan, O. Tulunay, S. Baltaci, *Int. Urol. Nephrol.* **2004**, *36*, 401.
- [47] S. Tsutsui, M. Kume, S. Era, *Breast Cancer* **2003**, *10*, 312.
- [48] S. F. Ngiow, A. Young, N. Jacquilot, T. Yamazaki, D. Enot, L. Zitvogel, M. J. Smyth, *Cancer Res.* **2015**, *75*, 3800.
- [49] S. L. Highfill, Y. Z. Cui, A. J. Giles, J. P. Smith, H. Zhang, E. Morse, R. N. Kaplan, C. L. Mackall, *Sci. Transl. Med.* **2014**, *6*, 237.
- [50] W. Hugo, J. M. Zaretsky, L. Sun, C. Y. Song, B. H. Moreno, S. Hu-Lieskovan, B. Berent-Maoz, J. Pang, B. Chmielowski, G. Cherry, E. Seja, S. Lomeli, X. J. Kong, M. C. Kelley, J. A. Sosman, D. B. Johnson, A. Ribas, R. S. Lo, *Cell* **2016**, *165*, 35.
- [51] Y. Zhu, B. L. Knolhoff, M. A. Meyer, T. M. Nywening, B. L. West, J. Q. Luo, A. Wang-Gillam, S. P. Goedegebuure, D. C. Linehan, D. G. DeNardo, *Cancer Res.* **2014**, *74*, 5057.
- [52] T. F. Gajewski, H. Schreiber, Y. X. Fu, *Nat. Immunol.* **2013**, *14*, 1014.
- [53] X. J. Liu, Y. Pu, K. Cron, L. F. Deng, J. Kline, W. A. Frazier, H. R. Xu, H. Peng, Y. X. Fu, M. M. Xu, *Nat. Med.* **2015**, *21*, 1209.
- [54] X. Y. Li, M. Wenes, P. Romero, S. C. C. Huang, S. M. Fendt, P. C. Ho, *Nat. Rev. Clin. Oncol.* **2019**, *16*, 425.
- [55] C. L. Chaffer, R. A. Weinberg, *Science* **2011**, *331*, 1559.